Composites: Part A 41 (2010) 360–368

Contents lists available at ScienceDirect

Composites: Part A

journal homepage: www.elsevier.com/locate/compositesa

Autonomic healing of low-velocity impact damage in fiber-reinforced composites

Amit J. Patel [a,b], Nancy R. Sottos [a,b], Eric D. Wetzel [c], Scott R. White [b,d,*]

[a] Department of Materials Science and Engineering, University of Illinois at Urbana-Champaign, 1304 W. Green St., Urbana, IL 61801, USA
[b] Beckman Institute for Advanced Science and Technology, University of Illinois at Urbana-Champaign, 405 N. Mathews Ave., Urbana, IL 61801, USA
[c] Materials Division, US Army Research Laboratory, AMSRD-ARL-WM-MA, Bldg. 4600, Aberdeen Proving Ground, MD 21005, USA
[d] Department of Aerospace Engineering, University of Illinois at Urbana-Champaign, Urbana, 104 S. Wright St., IL 61801, USA

ARTICLE INFO

Article history:
Received 15 July 2009
Received in revised form 4 November 2009
Accepted 8 November 2009

Keywords:
A. Self-healing materials
A. Polymer-matrix composites (PMCs)
B. Delamination
B. Impact behavior

ABSTRACT

In this study autonomic self-healing of impact damage in composite materials is shown using a microencapsulated healing agent. The components for self-healing, urea–formaldehyde microcapsules containing dicyclopentadiene (DCPD) liquid healing agent and paraffin wax microspheres containing 10 wt% Grubbs' catalyst, have been successfully incorporated in a woven S2-glass-reinforced epoxy composite. Low-velocity impact tests reveal that the self-healing composite panels are able to autonomically repair impact damage. Fluorescent labeling of damage combined with image processing shows that total crack length per imaged cross-section is reduced by 51% after self-healing. A testing protocol based on compression after impact reveals significant recovery of residual compressive strength (RCS) in self-healing panels. Self-healing panels show a higher threshold impact energy before RCS reduction, and as impact energy increases, RCS recovery decreases. Qualitative inspection shows that crack separation increases with increasing impact energy, indicating that self-healing performance depends on the ability to adequately fill damage volume.

1. Introduction

Because of their excellent in-plane properties and high specific strength, fiber-reinforced composites with polymeric matrices have found many uses in structural applications. Despite this success, they are particularly prone to damage from out-of-plane impact events. Although fiber damage is usually localized at the site of impact, matrix damage in the form of delaminations and transverse cracks can be more widespread. Delaminations, in particular, pose a serious issue because they can significantly reduce compressive strength [1–5] and grow in response to fatigue loading [2,6–9]. Adding to the problem, impact damage can be subsurface or barely visible, necessitating the use of expensive and time-consuming non-destructive inspection [2]. Once damage is located, there are many repair techniques that have been proposed or are currently practiced [10–13]. Most solutions rely on resin infiltration of delaminations or composite patches to provide load transfer across the damaged region. In cases of severe damage, damaged regions are removed and replaced with new composite material that is bonded or co-cured to the original material [10]. These repair techniques are generally time-consuming, complicated, and require unhindered access.

An alternative solution to manually repairing impact damage is the employment of self-healing materials. In particular, the strategy using microencapsulated healing agent, demonstrated by White and coworkers [14] and later modified by Rule et al. [15], has proven effective in repairing damage in polymeric matrices. The system requires adding two components to the epoxy matrix: microencapsulated monomer and wax microspheres containing Grubbs' catalyst. The wax microsphere approach has been found to provide more efficient distribution and utilization of catalyst particles than direct incorporation of catalyst particles. Autonomic self-healing occurs when matrix damage ruptures the microcapsules, releasing monomer into the crack plane, which then polymerizes in the presence of catalyst. This new polymer fills damage zones and bridges crack faces, typically resulting in partial or complete recovery of global mechanical properties. The autonomic nature of this approach eliminates the need for manual damage detection and repair processes. Initial studies on the recovery of mechanical properties in microencapsulated self-healing materials focused on monotonic fracture testing [14,16] and fatigue [17–19] of polymer composites without fiber reinforcement. In further work, Kessler et al. successfully incorporated the self-healing system into a woven fiber-reinforced composite and demonstrated recovery of Mode I interlaminar fracture toughness [20,21]. Additional studies by O'Brien et al. also used the Grub-

* Corresponding author. Address: Beckman Institute for Advanced Science and Technology, University of Illinois at Urbana-Champaign, 405 N. Mathews Ave., Urbana, IL 61801, USA. Tel.: +1 217 333 1077; fax: +1 217 244 0720.
E-mail address: swhite@illinois.edu (S.R. White).
URL: http://www.autonomic.uiuc.edu (S.R. White).

1359-835X/$ - see front matter © 2009 Elsevier Ltd. All rights reserved.
doi:10.1016/j.compositesa.2009.11.002

bs'-DCPD system and showed strength recovery in composite skin/stringer flange debond specimens [22].

Several other self-healing strategies in polymers have also been proposed. Chen et al. have developed a polymer that can repair cracks based on a thermally reversible Diels–Alder cross-linking reaction, allowing for re-mending upon heating [23]. Another solid-state system, demonstrated by Hayes and coworkers, utilizes a thermoplastic phase dissolved in an epoxy matrix [24]. Repair of cracks at elevated temperatures is believed to occur by crack bridging by thermoplastic polymer chains that have diffused to the site of damage. Yin and coworkers have also proposed a microencapsulated healing system with epoxy healing agent embedded in a woven fiberglass-reinforced epoxy composite containing latent imidazole curing agent [25,26]. Healing is accomplished at elevated temperature (140 °C) by the reaction of the microencapsulated epoxy with the unreacted imidazole curing agent. Systems based on the delivery of liquid healing agent from embedded tubes have also been proposed and investigated by several authors. This idea, proposed by Dry [27], was further investigated by Motuku et al. using glass pipettes and metal tubing [28]. Bleay et al. tested a composite composed of epoxy-filled hollow S2-glass fibers and demonstrated minor recovery of compression strength after impact [29]. Extending this work by using larger diameter hollow glass fibers selectively placed at key laminate interfaces, Bond and coworkers successfully demonstrated the repair of quasi-static and low-velocity impact damage to a carbon/epoxy laminate [30–33]. With the exception of the study by Pang and coworkers [30], the aforementioned healing systems are not autonomic; that is, they require some form of external intervention (temperature, heat, manual fluid injection, etc.) for healing and recovery. In the current study we demonstrate truly autonomic self-healing of impact damage in fiber-reinforced composites at ambient conditions.

Very few prior self-healing studies have investigated impact damage. In the studies using the hollow fiber approach [30–32], Bond and coworkers used quasi-static indentation to create damage similar to impact damage, and assessed damage recovery based on four-point bend experiments. More recently, Williams et al. [33] executed true compression after impact (CAI) experiments at 3 J, demonstrating 95% retention of CAI strength compared to 66% for unhealed panels. These materials, however, were not autonomically self-healing, requiring thermal treatments at 125 °C to enable CAI retention. Using the microencapsulated epoxy and latent curing agent approach, Yin and coworkers [26] measured CAI of woven fiberglass-reinforced epoxy composites impacted up to 3.5 J, showing improved healing performance at lower impact energies and through application of lateral pressure. However, healing in these systems was not autonomic, requiring heating to 140 °C. In another study, Williams et al. showed autonomic healing of impact damage to composite sandwich panels by delivering healing agent with hollow channels in the foam core [34]. However, the mechanical recovery seen in CAI tests was attributed to the restoration of core and core–skin interface properties rather than the healing of matrix damage in the fiber-reinforced composite skin.

In contrast, the present study demonstrates fully autonomic self-healing of low-velocity impact damage in a fiber-reinforced composite and explores impact behavior up to 45 J. Self-healing functionality is integrated in a conventional woven glass-reinforced epoxy composite based on the system described by White et al. [14] and later modified by Rule et al. [15] (Fig. 1). We visually examine the autonomic repair of impact-induced matrix damage in fiber-reinforced composites using a crack marking technique and direct observation of healed material. Mechanical recovery is assessed using a CAI testing protocol. The influences of impact energy and lateral pressure are investigated to study the effect of damage volume on healing performance.

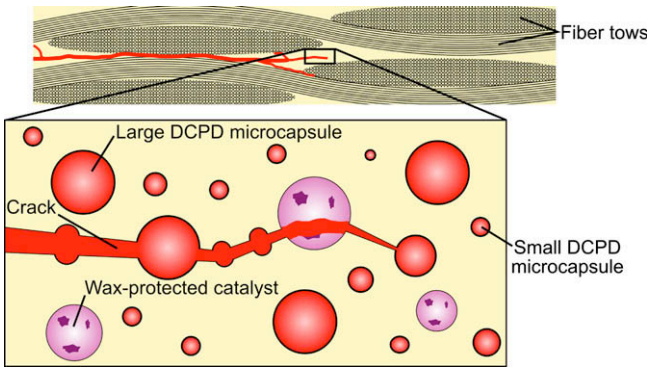

Fig. 1. Schematic of the self-healing system used in the matrix of a woven fiber-reinforced composite.

2. Materials

2.1. Self-healing components

The size scales of healing agent components incorporated into the composite system are a crucial design factor. Smaller components distribute more evenly and infiltrate into narrow interlaminar regions. However, because the amount of healing agent delivered to the crack plane varies linearly with microcapsule diameter [35], a reduction in size scale limits the amount of damage that can be healed. In addition, the efficiency of wax microspheres to protect the embedded catalyst diminishes with size as the surface area to volume ratio correspondingly increases [36].

Distilled *endo*-DCPD-filled microcapsules were manufactured by *in situ* poly(urea–formaldehyde) microencapsulation using the method described by Brown et al. [37]. Two different size ranges of microcapsules were employed to promote even distribution of microcapsules and ensure adequate delivery of DCPD healing agent to crack planes. Microcapsules of ~35 μm number average diameter were used to ensure even distribution and access to restricted locations, while microcapsules of ~125 μm number average diameter were used to provide a large supply of healing agent for delivery to damaged regions. Small microcapsules were made using an agitation rate of 1000 rpm and collecting microcapsules beneath the 75 μm sieve. Large microcapsules were made using an agitation rate of 550 rpm and collecting microcapsules between 125 μm and 250 μm sieves. The size distributions for both types of microcapsules are shown in Fig. 2a.

Wax-protected catalyst microspheres were made using a method similar to that described by Rule et al. [15], in which 10 wt% first generation Grubbs' catalyst (freeze-dried morphology [38]) was incorporated in paraffin wax microspheres. Plain paraffin wax microspheres were also fabricated for use in control specimens without self-healing functionality. A 0.2 wt% aqueous polyvinyl alcohol (average M_w 85,000–124,000, 87–89% hydrolyzed, Sigma–Aldrich) solution was used instead of the 0.28 wt% aqueous poly(ethylene-co-maleic anhydride) solution used previously [15].

Wax microsphere size is controlled by agitation rate. To keep the number density of microspheres in the final composite consistent, the average value of the microsphere diameter cubed was held constant. Catalyst-containing wax microspheres of 135 μm $\left(\langle d^3\rangle^{1/3}\right)$ were created at 1000 rpm. To achieve the same average diameter, plain wax microspheres were processed at 600 rpm. The size distributions of these wax microspheres are shown in Fig. 3a.

2.2. Composite materials, lay-up, and curing

Composite panels for low-velocity impact were nominally 101 × 101 × 4 mm and consisted of four plies of 24 oz/yd^2

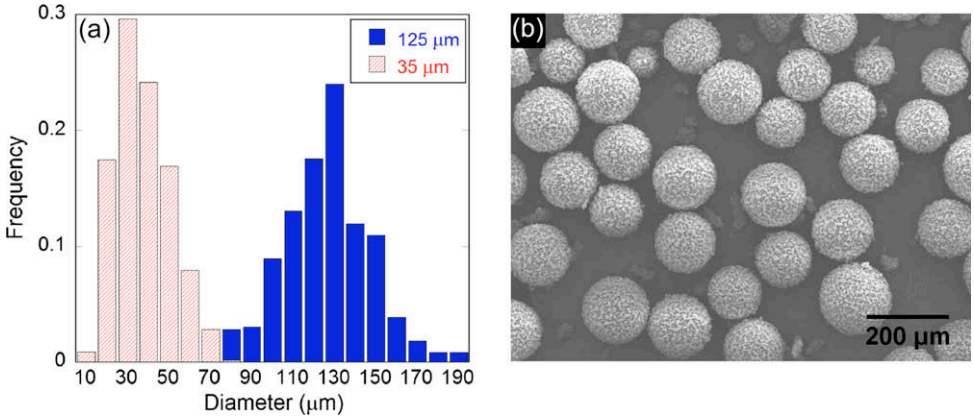

Fig. 2. (a) Histograms of microcapsule diameter for larger (125 μm) and smaller (35 μm) microcapsules used in this study. (b) SEM micrograph of larger DCPD microcapsules.

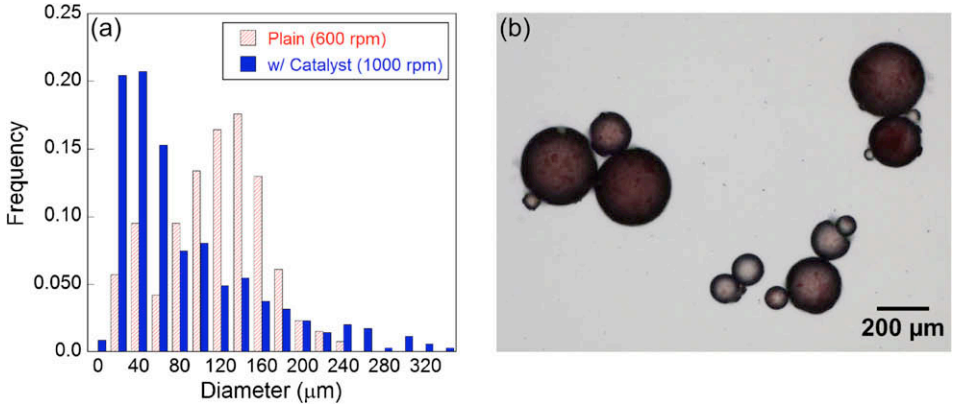

Fig. 3. (a) Histograms of diameter for plain wax microspheres and wax-encapsulated Grubbs' catalyst (10 wt%). (b) Optical micrograph of wax-encapsulated Grubbs' catalyst microspheres.

5 × 5 yarns/in. plain woven S2-glass fabric (Owens Corning Knytex SBA240F) in an Epon 862 and Epi-cure 3274 matrix (100:40 weight ratio). Self-healing (SH) panels were made with a 2:1 mass ratio of 35:125 μm DCPD-filled microcapsules, as well as catalyst-containing wax microspheres of 135 μm average diameter. Three types of control panels were employed in the experiments. Plain composite panels (C-I) contained no self-healing components. A second set of controls (C-II) contained only microcapsules at the standard 2:1 mass ratio of 35:125 μm size ranges. A final set of controls (C-III) contained both microcapsules and plain wax microspheres. A summary of panel compositions can be found in Table 1.

The resin matrix was prepared by mixing Epon 862 resin (286 g) with Epi-cure 3274 curing agent (114 g) and paraffin wax microspheres (10 g), together with healing agent microcapsules (33 g) in a 2:1 mass ratio of small to large capsules. The overall concentrations of microcapsules, microspheres, and active catalyst were 7.4 wt%, 2.3 wt%, and 0.23 wt%, respectively. Once mixed, the resin was partitioned into four equal portions, one for each layer of glass fabric, and degassed under vacuum before being used for lay-up.

Table 1
Summary of composite panel types.

Panel type	DCPD microcapsules	Wax microspheres
C-I	None	None
C-II	35 μm and 125 μm	None
C-III	35 μm and 125 μm	Plain, 135 μm
SH	35 μm and 125 μm	10 wt% Grubbs', 135 μm

The first portion of resin was laid down and spread evenly over the mold surface. A glass fabric layer was then placed on top and lightly rolled flat. The liquid epoxy was allowed to soak into the fabric rather than using pressure with the roller. This method was employed to avoid pushing and concentrating the self-healing components to the edge of the part. This process was repeated for the remaining layers. A porous peel ply, backed by bleeder cloth, was placed on the top surface to allow excess resin to bleed toward the top surface during compaction.

The samples were cured at room temperature for 24 h under compaction pressure, followed by 48 h at 35 °C with no pressure applied. Plain composite panels were compacted with 4.8 kPa pressure, while panels containing microcapsules and/or wax microspheres were compacted with 95.8 kPa of pressure. These compaction pressures yielded a final panel thickness of approximately 4 mm, and the fiber content was estimated, based on panel thickness, to be approximately 33% by volume for all panels. Increased compaction pressure was required for microcapsule-containing panels in order to maintain consistent overall laminate thicknesses. This effect is likely due to increased resin viscosity with the addition of microcapsules. The final concentrations of self-healing components in the composite panels were estimated to be approximately 0.13 g/cm^3 DCPD microcapsules and 0.039 g/cm^3 wax microspheres (0.0039 g/cm^3 Grubbs' catalyst) by assuming all self-healing components remained in the final composite panel. This assumption is reasonable because the self-healing components cannot bleed through the porous release ply. After curing, each large panel was then cut with a diamond saw into four smaller 101 mm × 101 mm panels.

3. Testing and characterization

3.1. Low-velocity impact testing

Impact testing was conducted on an Instron Dynatup 8200 instrumented drop-weight impact tester with the sample circularly clamped (76 mm diameter) and using a spherically shaped impact head of 25.4 mm radius of curvature. A schematic of the impact setup is shown in Fig. 4. Samples to be damaged were impacted with a range of energies as outlined in Table 2. Reported impact energy values are calculated from drop height and carriage mass values. For impact energies below 26.5 J, the lower limit on carriage mass required a reduction in drop height. Although this reduction lowers the impact velocity, the rate effects on impact damage are minor in this low-velocity impact regime [39]. The large curvature of the impact head, combined with this range of impact energies, produces matrix damage without significant fiber damage.

All impacted self-healing panels were given 48 h to heal before further testing. A majority of the SH panels were healed under ambient conditions: room temperature and no lateral pressure. However, a set of self-healing panels impacted with 45.1 J was healed with 1077 kPa lateral pressure applied using a hot-press in order to understand the effect of damage volume on healing performance. Corresponding C-III controls underwent the same conditions to separate any non-healing improvements in compressive strength due to damage compaction.

3.2. Damage imaging and quantification

Panels were sectioned through the point of impact into four quarters for imaging. Delaminations and matrix cracks exposed on the cross-section surface were marked by a fluorescent dye penetrant (Zyglo ZL-37) using a technique demonstrated by Kuboki et al. [40]. Fig. 5a shows a typical image of highlighted damage under UV illumination. For each panel, four separate images were obtained, one for each sectioning cut.

The total crack length per imaged edge was measured to quantify the degree of damage. First, cracks were manually traced with a pencil tool in Adobe Photoshop CS2. The resulting images were thresholded to yield just the crack tracings, which were in turn skeletonized using a Fovea Pro photo analysis plug-in (Fig. 5b). Finally, the total length of the skeleton was then computed using the same plug-in software.

3.3. Compression after impact

Compression after impact is a widely used test method to measure the residual compressive strength (RCS) of composites with impact damage. The RCS is sensitive to this type of damage due to localized buckling of sublaminates created by delaminations, leading to stress concentrations around the region of reduced stiffness [1,41–43]. CAI was used to assess the effect of self-healing components on composite performance and the degree of recovery due to the healing response.

CAI tests were conducted based on the ASTM standard D7137 [44]. However, the fixture was modified from the standard geometry to accommodate the 101 mm × 101 mm panels (Fig. 6). All panels underwent in-plane compression testing using a MTS 812 hydraulic test frame coupled with a Instron 8800 controller at a cross-head speed of 1 mm/min. Panels, both damaged and undamaged, were loaded until complete compressive failure across the width of the sample.

4. Results and discussion

4.1. Damage characterization

Self-healing panels impacted with the highest energy (45.1 J) show a 51% decrease in total crack length per imaged edge when compared to the corresponding C-III controls (Fig. 7). Plain composite panels (C-I) and microcapsule-only panels (C-II) were also tested to observe the effects of self-healing components on damage resistance. As shown in Fig. 7, there is a negligible increase in total crack length per imaged edge when plain panels are compared to microcapsule-only panels, indicating that the addition of the microcapsules does not significantly affect impact damage resistance. However, C-III panels show a significant jump in total crack length per edge, suggesting that the combination of wax microspheres and DCPD microcapsules has a detrimental effect on damage resistance. The addition of wax microspheres may be associated with a reduction in interlaminar shear properties, plasticization of the matrix, or they may act like voids within the matrix rich regions. Nevertheless, self-healing panels exhibit dramatically smaller crack length per imaged edge when compared to controls, indicating significant filling of damage with healed material.

Closer inspection of self-healing panels reveals poly-DCPD-filled delamination and transverse cracks, as well as unhealed sections (Fig. 8a). Healed delaminations are marked by a trail of poly-

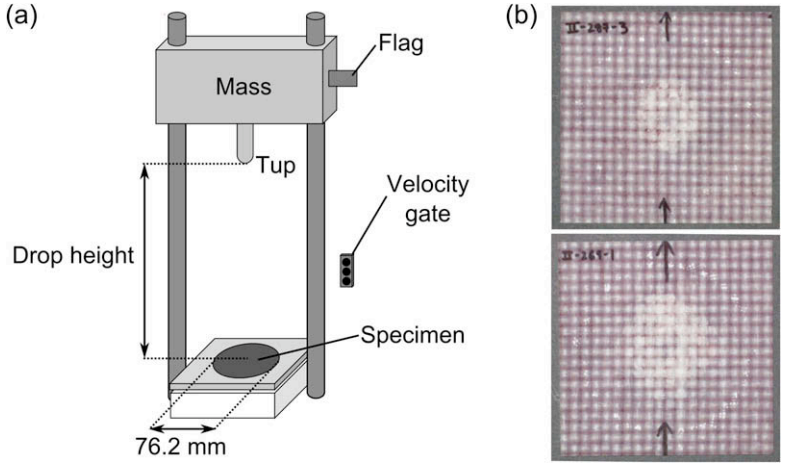

Fig. 4. (a) Schematic of drop-weight impact tower with instrumented tup. (b) Images of the backface of panels with damage from impacts of 22.2 J (top) and 45.1 J (bottom).

Table 2
Summary of composite panel impact and healing conditions. Reported impact energy values are calculated from drop height and carriage mass values. All panels were healed at room temperature (~24 °C).

Type	No. of samples	Drop mass (kg)	Drop height (m)	Impact energy (J)	Healing pressure (kPa)
C-I	8	0.00	0.00	0.0	0
	8	7.66	0.60	45.1	0
C-III	8	0.00	0.00	0.0	0
	4	4.52	0.30	13.3	0
	4	4.52	0.40	17.8	0
	4	4.52	0.50	22.2	0
	6	4.51	0.60	26.5	0
	6	5.58	0.60	32.9	0
	6	6.61	0.60	38.9	0
	8	7.66	0.60	45.1	0
	4	7.66	0.60	45.1	1077
SH	8	4.52	0.40	17.8	0
	7	4.52	0.50	22.2	0
	8	4.51	0.60	26.5	0
	4	5.58	0.60	32.9	0
	8	7.66	0.60	45.1	0
	8	7.66	0.60	45.1	1077

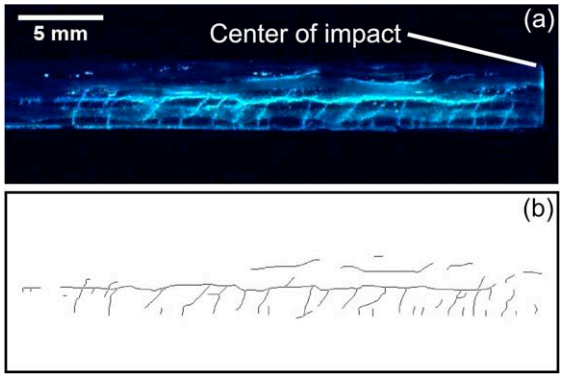

Fig. 5. (a) Image of fluorescently marked cracks under UV illumination. (b) Skeletonization of marked cracks.

DCPD-filled microcapsules that have ruptured onto the crack plane. C-III controls, on the contrary, do not show evidence of rebonded crack or delamination faces (Fig. 8b), as would be expected in the absence of catalyst.

4.2. Compression after impact results

Table 3 contains a summary of CAI test results for panels healed under ambient conditions. The RCS as a function of incident impact energy is plotted in Fig. 9 for self-healing and C-III controls. Both types of panels show typical RCS behavior [45] with a threshold impact energy below which little or no drop in RCS is detected. Self-healing panels show nearly twice the threshold energy of C-III panels. Above their respective threshold energies, both types of panels show a reduction in RCS with increasing impact energy. For self-healing panels, this drop-off in performance appears to be faster, and by 45.1 J of impact energy, the RCS's for self-healing and C-III panels are nearly the same.

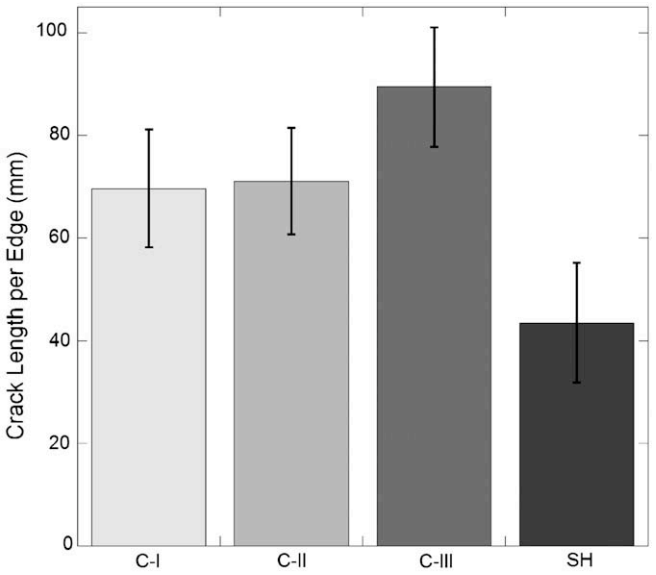

Fig. 7. Total crack length per imaged edge for plain (C-I), microcapsule-only (C-II), microcapsule and microsphere (C-III), and self-healing (SH) composite panels impacted with 45 J. Error bars are ±1 standard deviation.

The model developed by Caprino [46] for the strength of notched composite panels has also been generalized for compression after impact [45,47] such that RCS, σ_r, is related to impact energy, U, by the power law

$$\frac{\sigma_r}{\sigma_0} = \left(\frac{U_0}{U}\right)^{\beta}, \tag{1}$$

where σ_0 is the undamaged compressive strength and U_0 is the threshold impact energy. The more convenient form

$$\log \sigma_r = \log \sigma_0 + \beta(\log U_0 - \log U) \tag{2}$$

can be used to fit experimental data. For analyzing the data in this study, σ_0 was taken as the average compressive strength of all undamaged C-III panels. The parameters U_0 and β were found by performing a least-squares fit of Eq. (2) to the average measured RCS at each energy level. For C-III controls, panels impacted with 17.8 J or more were used. For the self-healing case, fittings were performed both for the full set of data and by excluding the data at 17.8 J. The fit was significantly better when excluding the 17.8 J data (standard deviation of residuals of 1.09 MPa versus 2.28 MPa), so the resulting U_0 and β values for this fit are reported here. This result suggests that 17.8 J is below the threshold impact

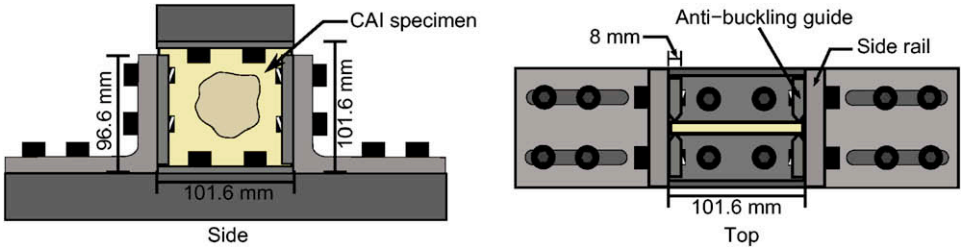

Fig. 6. Schematic of compression after impact fixture.

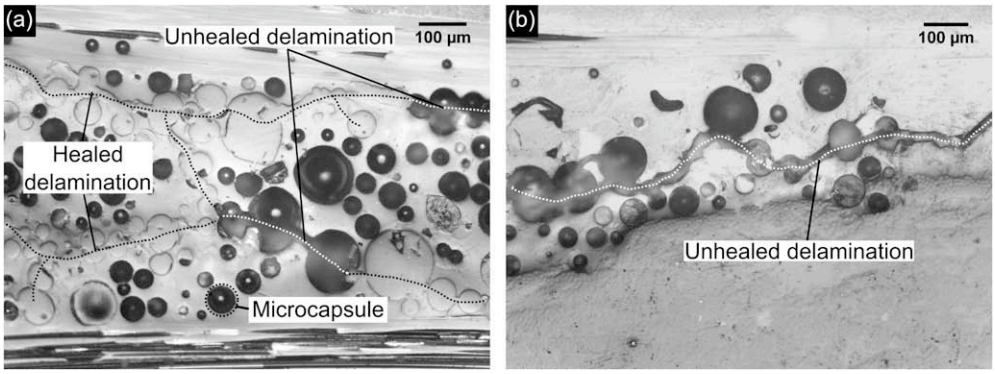

Fig. 8. Optical micrographs of cross-sections of (a) a partially healed section of delamination in a self-healing panel impacted with 45.1 J and (b) a section of unhealed delamination in a C-III non-healing control panel impacted with 45.1 J.

Table 3
Summary of CAI test results for panel groups healed under ambient conditions. Errors reported are ±1 standard deviation.

Type	Impact energy (J)	Compressive strength (MPa)	Maximum tangent stiffness (GPa)	Average stress at maximum tangent stiffness (MPa)
C-I	0.0	80 ± 5.1	11.7 ± 0.29	48 ± 8.9
	45.1	72 ± 2.8	11.3 ± 0.37	38 ± 7.7
C-III	0.0	82 ± 4.6	11.2 ± 0.26	49 ± 7.0
	13.3	80 ± 7.2	11.7 ± 0.17	45 ± 5.1
	17.8	68 ± 1.6	11.4 ± 0.15	34 ± 1.9
	22.2	67 ± 6.9	10.8 ± 0.13	33 ± 1.3
	26.5	64 ± 5.9	10.6 ± 0.35	34 ± 2.6
	32.9	59 ± 2.9	10.8 ± 0.53	31 ± 10
	38.9	60 ± 4.9	10.8 ± 0.52	30 ± 2.0
	45.1	55 ± 2.4	9.8 ± 0.39	27 ± 3.5
SH	17.8	79 ± 6.5	11.4 ± 0.23	47 ± 5.5
	22.2	76 ± 6.7	11.4 ± 0.31	44 ± 7.5
	26.5	71 ± 5.9	10.7 ± 0.28	40 ± 7.0
	32.9	66 ± 2.7	11.2 ± 0.13	35 ± 1.6
	45.1	56 ± 4.7	10.0 ± 0.38	32 ± 3.5

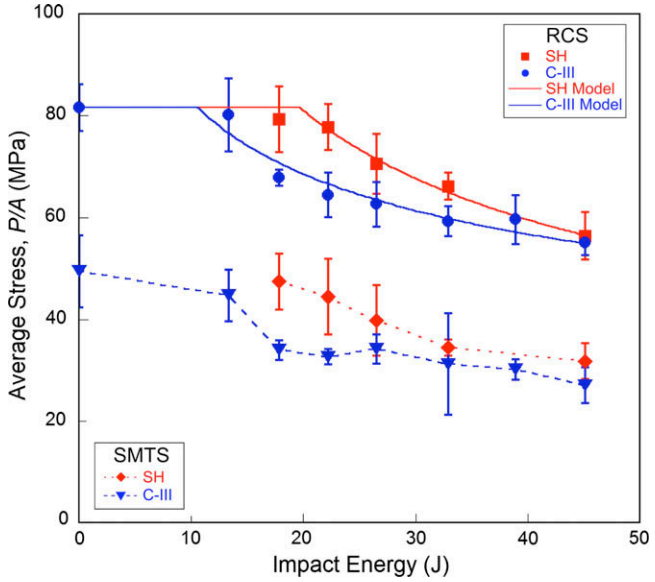

Fig. 9. Residual compressive strength (RCS) and average stress at maximum tangent stiffness (SMTS) for non-healing control panels (C-III) and self-healing panels (SH) versus nominal incident impact energy. Error bars are ±1 standard deviation. Also plotted is a fit to RCS based on a model from [47].

energy for the SH case. In fact, six of the eight SH panels impacted at this energy healed to at least 97% of the average undamaged C-III RCS.

Based on the model fitting results, threshold impact energy, U_0, for self-healing panels (19.7 J) is almost twice that of C-III panels (10.7 J). The exponent β, which is related to how fast RCS drops off with increasing impact energy, is larger for self-healing panels (0.44) than for C-III panels (0.28), indicating a reduction in self-healing recovery with increasing impact energy. However, because of the sensitivity of U_0 and β to experimental error, additional experimental data is required to definitively quantify these trends.

The better recovery of RCS at lower energies is likely the result of decreased damage volume. Optical images of cross-sections of impacted C-III composites reveal that delamination separation increases with increasing impact energy. Fig. 10 shows examples of the largest delamination separations observed for C-III panels impacted with 45.1 J and 17.8 J. Clearly, C-III panels impacted with 45.1 J possess considerably more damage separation than those impacted with 17.8 J. C-III panels impacted with 45.1 J can have delamination separations of approximately 100 μm, whereas the largest delamination separations seen in C-III panels impacted with 17.8 J are approximately 35 μm.

In a manner similar to that by Rule and coworkers [35], the theoretical volume of healing agent released for planar cracks can be estimated as

$$V_h = \Phi_c d_c A, \tag{3}$$

where Φ_c is the local volume fraction of microcapsules, d_c is microcapsule diameter, and A is the area of crack created. For complete filling of the damage volume, $V_h = At$, where t is the separation distance of the crack. Thus,

$$t = \Phi_c d_c \tag{4}$$

is the maximum average crack separation distance for which complete filling of damage is possible. For two sizes of microcapsules, t can be calculated separately for each size and then added. Thus Eq. (4) becomes

$$t = \Phi_{c,1} d_{c,1} + \Phi_{c,2} d_{c,2}. \tag{5}$$

For the case of a 2:1 mass ratio of 35:125 μm microcapsules, $\Phi_{c,1} = 0.66\Phi_c$ and $\Phi_{c,2} = 0.33\Phi_c$, assuming the densities of the microcapsules are equal. Since microcapsules concentrate in interlaminar regions, an estimate of the local concentration of microcapsules in these regions is needed to calculate Φ_c. This concentration, estimated by measuring the area fraction of microcapsules in a thresholded cross-sectional image, is ~0.35. Thus, the maximum average crack separation distance $t = 23$ μm. In the case of panels impacted with 45.1 J, where much of the damage is on

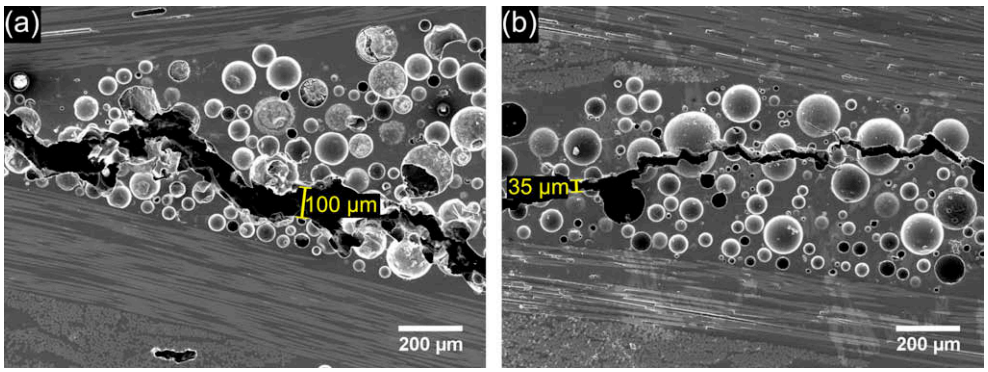

Fig. 10. Examples of the largest delamination separations seen in C-III panels impacted with (a) 45.1 J and (b) 17.8 J.

the order of 100 μm, most damage will not be filled or healed. For panels impacted at 17.8 J, almost all of the damage separations are significantly smaller than 35 μm and should be completely filled by poly-DCPD. Thus, as impact energy increases, damage separation increases, filling of the damage with healing agent decreases, and RCS recovery is expected to decrease. These results agree with the key finding by Rule and coworkers [35] that healing efficiency in tapered double cantilever beam specimens is reduced with decreasing amounts of delivered healing agent.

Although SH panels impacted with 45.1 J show little recovery of RCS when compared to C-III controls, their mechanical behavior is not identical to C-III controls. Fig. 11 shows compression loading curves for an undamaged C-III panel, a C-III panel impacted with 45.1 J, and a SH panel impacted with 45.1 J. Average stress, load divided by the panel cross-sectional area, is plotted versus displacement normalized to panel height. For the undamaged C-III control, there is an initial softness in loading associated with the specimen settling in the grips, followed by a region of fairly constant tangent stiffness. Near failure this panel quickly decreases in tangent stiffness until eventual compressive failure marked by a sudden load drop. In contrast, impacted C-III controls deviate from undamaged behavior at fairly low loads with a gradual reduction in tangent stiffness until final compressive failure. This behavior is likely the result of local buckling in the damaged region. Local buckling of the damaged region leads to a zone of reduced stiffness [42], which reduces overall panel tangent stiffness. Thus, for C-III panels the deviation from undamaged behavior marks the onset of local buckling of sublaminates.

In contrast, self-healing panels impacted at 45.1 J show a markedly different behavior than corresponding C-III controls. Unlike C-III panels, self-healing panels replicate the behavior of undamaged C-III panels to much higher loads, before a rapid degradation in tangent stiffness and then eventual compressive failure at load levels similar to damaged C-III panels. The similarity in loading behavior between self-healing panels and undamaged C-III panels is likely due to self-healing material bonding delamination faces together and delaying local buckling of the sublaminates. However, at a critical level of load, adhered delamination faces reopen, and the tangent stiffness of the panel rapidly decreases. The key differences in behavior among undamaged and impacted C-III controls and impacted self-healing panels can be more clearly seen in tangent stiffness versus average stress plots (Fig. 12).

To quantify this difference in panel stiffness behavior, average stress at maximum tangent stiffness (SMTS) was used as a metric

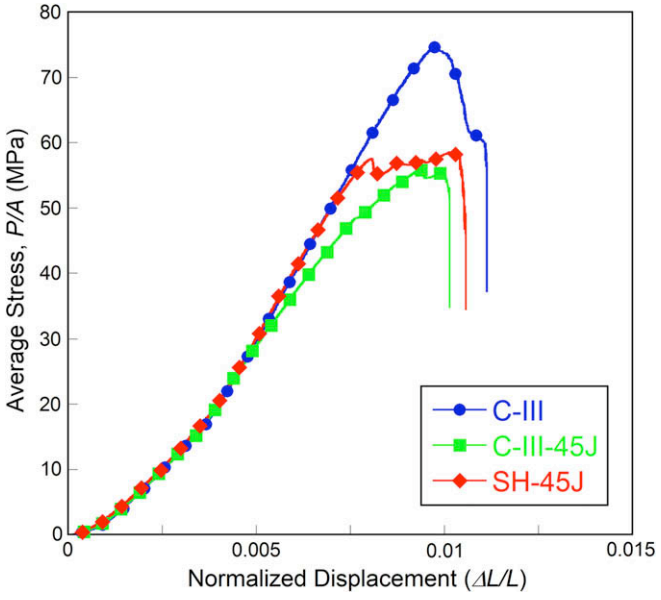

Fig. 11. Representative CAI loading curves (average stress versus normalized displacement) for undamaged and impacted (45.1 J) C-III control panels and impacted (45.1 J) self-healing composite panels.

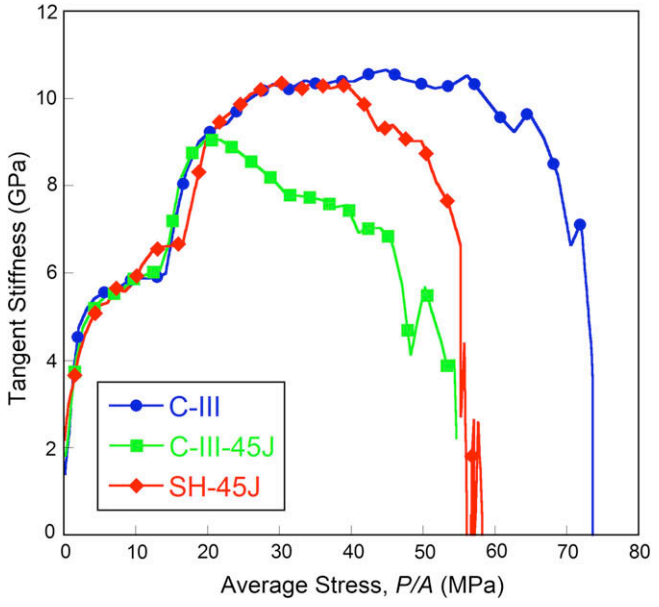

Fig. 12. Representative tangent stiffness versus average stress curves (corresponding to Fig. 11) for undamaged and impacted (45.1 J) C-III control panels and impacted (45.1 J) self-healing composite panels.

of mechanical performance, since it corresponds to the onset of degradation in mechanical properties. SMTS decreases with increasing impact energy for C-III controls, as shown in Fig. 9. Self-healing panels, however, consistently show higher SMTS, even up to the highest impact energy tested. These results suggest a delay in local buckling due to healing and adhesion of delamination faces.

To further investigate the effect of damage volume on healing performance, a set of self-healing panels was healed under lateral pressure. Lateral pressure is expected to reduce separation of delamination faces and damage volume, and thus increase RCS recovery [26]. Self-healing panels healed under lateral pressure (1077 kPa) showed increased RCS (Table 4), approximately 78% of their original compressive strength compared to 68% for panels healed without pressure. Two of the eight panels healed under pressure recovered to 93% and 95% of the average compressive strength of undamaged C-III panels. Additionally, panels healed under pressure consistently showed significantly higher SMTS (Table 4), further evidence of improved self-healing performance. A set of control panels (C-III) which underwent the same "healing" conditions under pressure showed no increase in RCS or SMTS (Table 4).

Also of interest is the mechanical degradation caused by addition of self-healing components. As previously discussed, it was found that the combination of both DCPD microcapsules and wax microspheres reduced the damage resistance of panels subject to low-velocity impact. In addition, it has been shown that microcapsule addition reduces the effective tensile strength of the matrix [48,49]. However, comparisons of RCS of undamaged C-I and C-III controls (Table 3) show the self-healing components in C-III panels do not reduce in-plane compressive strength. Similarly, no significant difference is seen for SMTS. Since compressive failure in woven laminates can be initiated by fiber microbuckling and kinking in the fiber-rich regions [50,51], it is possible that because the self-healing components are segregated in the interlaminar regions, they do not appreciably affect this failure process. Thus, the addition of self-healing components, which reduces damage resistance, does not have a deleterious effect on undamaged in-plane compressive properties obtained using the CAI fixture. This behavior may not be reflective of other composite materials more sensitive to fiber alignment, such as laminates made from unidirectional plies.

5. Conclusion

In this study we have demonstrated autonomic self-healing of impact damage in composite materials for the first time using a microencapsulated approach. Fluorescent labeling of matrix damage combined with image processing shows a significant decrease in observed crack length when comparing impacted self-healing panels to impacted control panels. Furthermore, the addition of microcapsules to the matrix of the composite had little effect on impact damage resistance, while the additional incorporation of wax microspheres increased impact damage considerably. This reduction in damage resistance due to the presence of wax microspheres is an important limitation that should be addressed in future self-healing systems.

Using a protocol based on CAI testing, self-healing panels showed recovery in average stress at maximum tangent stiffness and residual compressive strength. CAI results indicate that self-healing increases the threshold impact energy by nearly twofold compared to non-self-healing controls. Self-healing panels healed under lateral pressure showed greater recovery of residual compressive strength and average stress at maximum tangent stiffness, due to more complete filling of damage volume. The results of this study demonstrate the potential for significant mechanical recovery of damage in impacted composites when complete filling of damage is feasible with the microencapsulated self-healing material approach. Conversely, these results also indicate that autonomic self-healing in impacted composites can be enhanced by increasing the delivery volume of healing agent to the damage zone, or by reducing the damage volume induced by impact.

Table 4
Summary of CAI test results for panels impacted with 45.1 J with and without pressure during healing period. Errors reported are ±1 standard deviation.

Type	Healing pressure (kPa)	Compressive strength (MPa)	Average stress at maximum tangent stiffness (MPa)
C-III	0	55 ± 2.4	27 ± 3.5
	1077	54 ± 5.0	27 ± 4.1
SH	0	56 ± 4.7	32 ± 3.5
	1077	64 ± 10	40 ± 6.2

Acknowledgments

Funding for this project is provided by the US Army Research Laboratory (ARL). The authors would like to thank Seth Ghiorse and Dan Baechle of ARL for helpful discussions. The authors would also like to thank John D. Williams and the Materials Testing Instructional Laboratory at the University of Illinois (UI) for use of the drop-weight impact tester. Other facilities used at UI include the Advanced Materials Testing and Engineering Laboratory, the Composites Manufacturing Laboratory, and the Beckman Institute for Advanced Science and Technology. Electron microscopy was carried out in the Center for Microanalysis of Materials at UI, which is supported by the U.S. Department of Energy.

References

[1] Zhou G, Greaves LJ. Damage resistance and tolerance of thick laminated woven roving GFRP plates subjected to low velocity impact. In: Reid R, Zhou G, editors. Impact behavior of fibre-reinforced composite materials. Cambridge: Woodhead Publishing Ltd. and CRC Press LLC; 2000.
[2] Baker AA, Jones R, Callinan RJ. Damage tolerance of graphite/epoxy composites. Compos Struct 1985;4(1):15–44.
[3] Prichard JC, Hogg PJ. The role of impact damage in post-impact compression testing. Composites 1990;21(6):503–11.
[4] Guild FJ, Hogg PJ, Prichard JC. A model for the reduction in compression strength of continuous fibre composites after impact damage. Composites 1993;24(4):333–9.
[5] Xiong Y, Poon C, Straznicky PV, Vietinghoff H. A predictive method for the compressive strength of impact damaged composite laminates. Compos Struct 1995;30(4):357–67.
[6] Chen AS, Almond DP, Harris B. Impact damage growth in composites under fatigue conditions monitored by acoustography. Int J Fatigue 2002;24(2–4):257–61.
[7] Konishi DY, Johnston WR. Fatigue effects on delaminations and strength degradation in graphite/epoxy laminates. In: Composite materials: testing and design (fifth conference) conference proceedings, New Orleans, (LA, USA): ASTM; 1978. p. 597–619.
[8] Mitrovic M, Hahn HT, Carman GP, Shyprykevich P. Effect of loading parameters on the fatigue behavior of impact damaged composite laminates. Compos Sci Technol 1999;59(14):2059–78.
[9] Ramkumar RL. Effect of low-velocity impact damage on the fatigue behavior of graphite/epoxy laminates. In: Long-term behavior of composites conference proceedings, Williamsburg, VA, USA: ASTM. p. 116–35.
[10] Myhre SH, Labor JD. Repair of advanced composite structures. J Aircraft 1981;18(7):546–52.
[11] Heslehurst RB. Challenges in the repair of composite structures—part I. SAMPE J 1997;33(5):11–6.
[12] Heslehurst RB. Challenges in the repair of composite structures—part II. SAMPE J 1997;33(6):16–21.
[13] Dorworth L, Gardiner G, Training A. Repair of composite structures—a review. J Adv Mater 2007;39(4):3–13.
[14] White SR, Sottos NR, Geubelle PH, Moore JS, Kessler MR, Sriram SR, et al. Autonomic healing of polymer composites. Nature 2001;409(6822):794–7.
[15] Rule J, Brown EN, Sottos NR, White SR, Moore JS. Wax-protected catalyst microspheres for efficient self-healing materials. Adv Mater 2005;17(2):205–8.

[16] Brown EN, Sottos NR, White SR. Fracture testing of a self-healing polymer composite. Exp Mech 2002;42(4):372–9.
[17] Brown EN, White SR, Sottos NR. Retardation and repair of fatigue cracks in a microcapsule toughened epoxy composite—part I: manual infiltration. Compos Sci Technol 2005;65(15):2466–73. Special Anniversary Issue.
[18] Brown EN, White SR, Sottos NR. Retardation and repair of fatigue cracks in a microcapsule toughened epoxy composite. Part II: Manual infiltration. Compos Sci Technol 2005;65(15):2474–80. Special Anniversary Issue.
[19] Jones AS, Rule JD, Moore JS, Sottos NR, White SR. Life extension of self-healing polymers with rapidly growing fatigue cracks. J R Soc Interface 2007;4(13):395–403.
[20] Kessler MR, White SR. Self-activated healing of delamination damage in woven composites. Composites Part A 2001;32(5):683–99.
[21] Kessler MR, Sottos NR, White SR. Self-healing structural composite materials. Composites Part A 2003;34(8):743–53.
[22] O'Brien TK, White SR. Assesment of composite delamination self-healing via micro-encapsulation. In: American society for composites 23rd technical conference proceedings. Memphis, (TN, USA): DEStech Publications, Inc. p. 116–35.
[23] Chen X, Wudl F, Mal AK, Shen H, Nutt SR. New thermally remendable highly crosslinked polymeric materials. Macromolecules 2003;36(6):1802–7.
[24] Hayes SA, Jones FR, Marshiya K, Zhang W. A self-healing thermosetting composite material. Composites Part A 2007;38(4):1116–20.
[25] Yin T, Zhou L, Rong MZ, Zhang MQ. Self-healing woven glass fabric/epoxy composites with the healant consisting of micro-encapsulated epoxy and latent curing agent. Smart Mater Struct 2008;17(1):1–8.
[26] Yin T, Rong MZ, Wu J, Chen H, Zhang MQ. Healing of impact damage in woven glass fabric reinforced epoxy composites. Composites Part A 2008;39(9):1479–87.
[27] Dry C. Procedures developed for the self repair of polymer matrix composite materials. Compos Struct 1996;35(3):263–9.
[28] Motuku M, Vaidya UK, Janowski GM. Parametric studies on self-repairing approaches for resin infused composites subjected to low velocity impact. Smart Mater Struct 1999;8(5):623–38.
[29] Bleay SM, Loader CB, Hawyes VJ, Humberstone L, Curtis PT. A smart repair system for polymer matrix composites. Composites Part A 2001;32(12):1767–76.
[30] Pang J, Bond IP. A hollow fibre reinforced polymer composite encompassing self-healing and enhanced damage visibility. Compos Sci Technol 2005;65(11):1791–9.
[31] Trask RS, Bond IP. Biomimetic self-healing of advanced composite structures using hollow glass fibres. Smart Mater Struct 2006;15(3):704–10.
[32] Williams GJ, Trask RS, Bond IP. A self-healing carbon fibre reinforced polymer for aerospace applications. Composites Part A 2007;38(6):1525–32.
[33] Williams GJ, Bond IP, Trask RS. Compression after impact assessment of self-healing CFRP. Composites Part A 2009;40(9):1399–406.
[34] Williams HR, Trask RS, Bond IP. Self-healing sandwich panels: restoration of compressive strength after impact. Compos Sci Technol 2008;68(15–16):3171–7.
[35] Rule J, Sottos NR, White SR. Effect of microcapsule size on the performance of self-healing polymers. Polymer 2007;48(12):3520–9.
[36] Wilson GO, Moore JS, White SR, Sottos NR, Andersson HM. Autonomic healing of epoxy vinyl esters via ring opening metathesis polymerization. Adv Funct Mater 2008;18(1):44–52.
[37] Brown EN, Kessler MR, Sottos NR, White SR. In situ poly(urea formaldehyde) microencapsulation of dicyclopentadiene. J Microencapsulation 2003;20(6):719–30.
[38] Jones AS, Rule JD, Moore JS, White SR, Sottos NR. Catalyst morphology and dissolution kinetics of self-healing polymers. Chem Mater 2006;18(5):1317.
[39] Robinson P, Davies GAO. Impactor mass and specimen geometry effects in low velocity impact of laminated composites. Int J Impact Eng 1992;12(2):189–207.
[40] Kuboki T, Hilvo T, Jar PYB. Detection of interlaminar cracks in fiber-reinforced polymers. J Mater Sci Lett 2002;21(22):1789–91.
[41] Abrate S. Impact on laminated composite materials. Appl Mech Rev 1991;44(4):155–90.
[42] Abrate S. Impact on laminated composites: recent advances. Appl Mech Rev 1991;47(11):517–44.
[43] Freitas MD, Reis L. Failure mechanisms on composite specimens subjected to compression after impact. Compos Struct 1998;42(4):365–73.
[44] ASTM international compressive residual strength properties of damaged polymer matrix composite materials, test method designation: D 7137/D 7137M-05.
[45] Hirai Y, Hamada H, Kim JK. Impact response of woven glass-fabric composites—I. Effect of fibre surface treatment. Composites Part A 1998;58(1):91–104.
[46] Caprino G. On the prediction of residual strength for notched laminates. J Mater Sci 1983;18(8):2269–73.
[47] Caprino G. Residual strength prediction of impacted CFRP laminates. J Compos Mater 1984;18(6):508–18.
[48] Blaiszik BJ, Sottos NR, White SR. Nanocapsules for self-healing materials. Compos Sci Technol 2008;68(3–4):978–86.
[49] Rzesutko AA, Brown EN, Sottos NR. Tensile properties of self-healing epoxy. TAM Tech Report 2003:1041–55.
[50] Reifsnider AL, Mirzadeh F. Compressive strength and mode of failure of 8H Celion 3000/PMR15 woven composite material. J Compos Tech Res 1988;10(4):156–64.
[51] Fleck NA, Jelf PM, Curtis PT. Compressive failure of laminated and woven composites. J Compos Tech Res 1995;17(3):212–20.